CHAPTER 5

FABRICATION OF FREE-STANDING MICROPATTERNED POLYSTYRENE-ALUMINA HYBRID FILMS WITH AMINO-FUNCTIONALISED BF CAVITIES

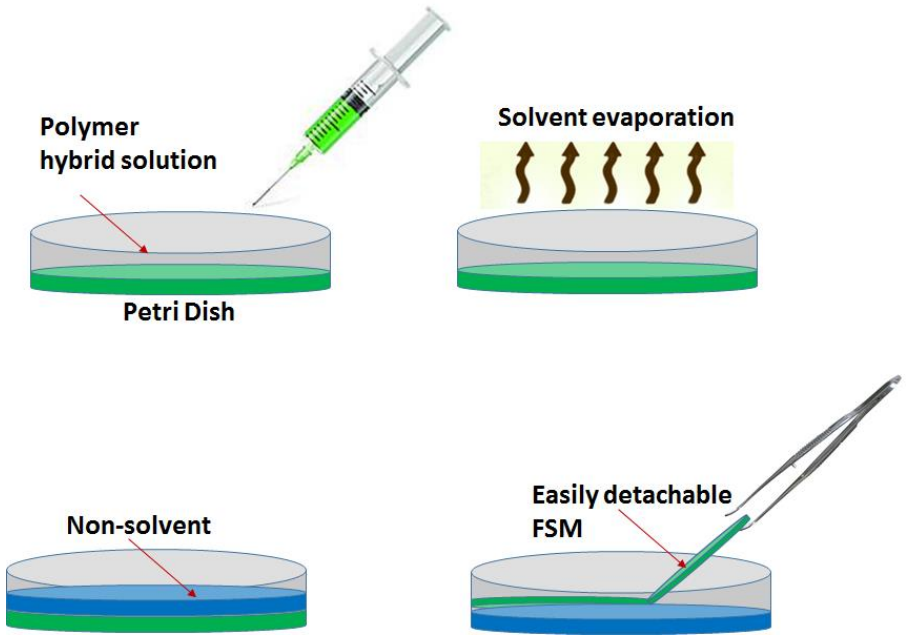

5.1. ABSTRACT

Free-standing micropatterned polystyrene-alumina hybrid films with amino-functionalized breath figure cavities (amino-FSM) have been fabricated by simple casting of polystyrene/amino-functionalized amphiphilic alumina (SA) particles suspension in chloroform (PSA/CFM) in to a petri dish and allowing the solvent to evaporate off under ambient conditions. The amino-FSM film can be removed easily from the substrate by pouring a non-solvent of the polymer into the petri dish. The hybrid films were found to be consisted of breath figure cavities throughout the film surface. The tuning of pore morphology was carried out by varying the thickness of the film as well as the SA particle concentrations. We observed a variation in cavity size and feature density with thickness of the films and particle concentration. The

presence of active amino groups inside the BF cavities were qualitatively and quantitatively estimated by analysing the florescent activated FSM films using fluorescamine. The FSM exhibited enhanced thermal and mechanical property owing to the presence of alumina particles. The present method opens up a simple route for the fabrication of FSM with functionalized BF cavities for many advanced applications.

5.2. INTRODUCTION

Micropatterned films have been of great research interest due to their many advanced applications. There are supported and free standing micropatterned films (FSMs). The drop casting is the generally adopted method for the supported patterned film. However, the supported films find difficulty in removing from the substrate. FSM could overcome these difficulties and can be implemented as such without any support for many industrial applications. Free-standing micropatterned films are well-suited for many chemical and biological applications due to their flexibility, easy handling, and ease of post-modification to induce various functionalities. Functionalized FSM have added advantages because of their topography and controlled surface properties which enables them to be used for the patterning of biomolecules like proteins, DNA, etc. Many multi-step processes were developed for the fabrication of functionalized FSM such as photolithographic methods, templating methods etc. Breath Figure technique which utilizes the mobile templates of water droplets that condenses on the cold surface of polymer solution opens a cheap and time consuming process for the fabrication of functionalized FSM. The functionalities can be induced either '*in-situ*' method or by the post modification of pre-fabricated FSM. The incorporation of inorganic nanoparticles into the BF cavity

of FSM opens a straightforward routes for the functionality enrichment inside the cavity. An added advantage of these hybrid films are the enhanced mechanical strength and improved thermal and optical properties. The unique properties of the nanoparticles can be effectively utilised. The BF mechanism operating in the hybrid FSM were assisted by inorganic nanoparticles by a process called "Pickering emulsion". These particles can be modified to attain desired functionality to the BF cavity.

Among the general methods of preparation of FSM, the most common method is the spreading of polymer solution on water surface. The interfacial tension between the polymer solution and the water surface were reduced by the presence of a surfactant monolayer. Nishikawa et al. fabricated FSM polymer film, but the method was limited to amphiphilic co-polymers (*Nishikawa et al., 2002*). Hongmin Ma et al *(Ma et al., 2011*) have reported the fabrication of FSM film from polystyrene and sterically stabilized AuNPs by casting the chloroform solution of polymer and particle onto the water surface containing surfactant monolayer in open air. They obtained BF cavities with asymmetric through-pore structure. However, the films fabrication by 'spreading on water surface' required a surface-active amphiphilic polymers.

Another strategy in the development of large area ordered honeycomb structures was put forward by Huang et al. by fabricating patterned PMMA and PS dishes without the use of external polymer solution (*Huang et al., 2014; Tu et al., 2014*). Cheng et al. fabricated BF patterned film from amphiphilic dendronized block copolymer by 'on-solid spreading' method and 'on-water spreading' method and comparison of these two methods revealed that small sized cavities with larger

surface density were obtained by spreading on water but with lower regularity (*Cheng et al., 2005*).

In the previous chapters, we had discussed the formation of breath figures on the drop cast residue and studied the various parameters that influence the breath figure morphology. These drop cast films were prepared on the glass substrate and were difficult to separate from the substrate without damaging the film. In this present chapter, we demonstrated a simple and straight forward route to fabricate FSM films by casting polystyrene-alumina suspensions in chloroform into a petri dish and allowed to evaporate off the solvent. The deposition of much large volume on a petri dish (3.5 cm dia.) produced films having BF patterns in large area and were found to be easily detachable from the petri dish. Through our work the BF patterns formed on the films were analysed and morphological tuning was carried out by changing the thickness of the film and the particle concentration.

5.3. EXPERIMENTAL

5.3.1. Materials

The materials used were amino-functionalised amphiphilic alumina nano particles (synthesized), Polystyrene (GPPS, Mw ~3.6K, PI=1.6) and Chloroform (Synthetic reagents, Merck Specialties Pvt. Ltd., India).

5.3.2. Fabrication of Free Standing (FSM) film

The amino-functionalised amphiphilic-alumina particle with hydrophobic/hydrophilic balance of 4 (termed as 4SA) was used for FSM preparation. The synthesis of 4SA particles was described in section 2.3.2. FSM film was prepared by dispersing desired amount of 4SA particles in 15 mg/mL of polystyrene/chloroform (PS/CFM) solution and sonicating for 10min. The

suspension (PSA suspension) thus obtained was poured into a glass petri dish of 3.5 cm diameter and allowed to dry under ambient conditions (temperature of 28-30 °C and relative humidity of 70-80 %). The film was post dried in an air oven at 60 °C. The volume of the suspension was varied from 0.2 ml to 1.5 ml. The film was separated from the petri dish by pouring methanol into the petri dish so that the film got detached from the dish. It was then wiped and dried in an air oven at 60 °C.

5.4. RESULTS AND DISCUSSIONS

The FSM film was semi-transparent and flexible. Figure 5.1. (A) shows the photograph of FSM kept inside with the petri dish used for the film preparation. The inset of the figure 5.1. (A) proves its semi-transparent nature. Figure 5.1 (B-E) shows the optical microscopic images of the FSM taken at different regions, from edge to centre.

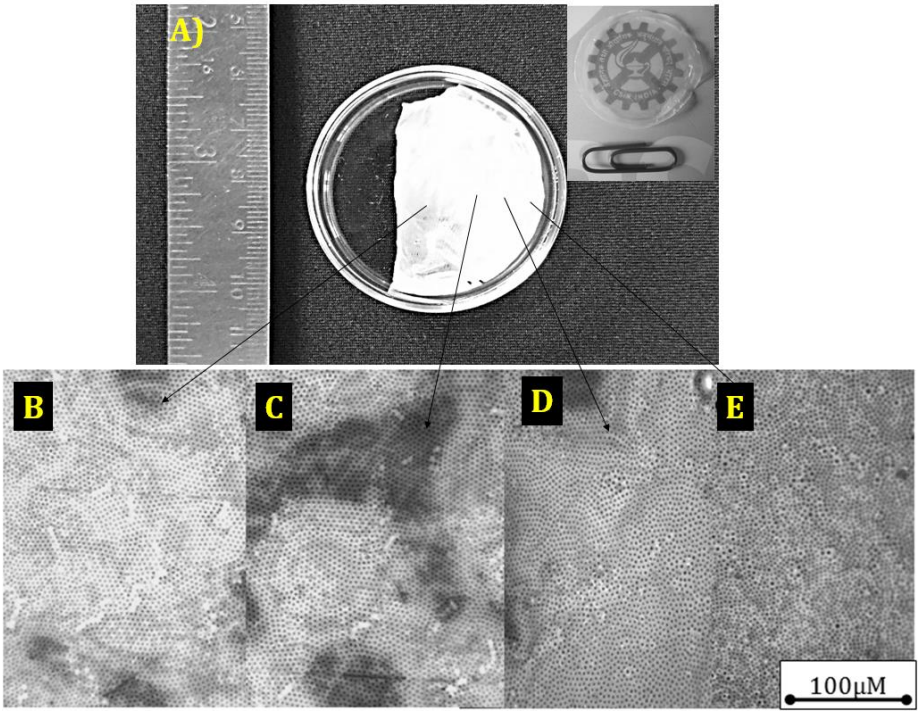

Figure 5.1. (A). Digital photograph of the FSM. (B-E) Optical microscopic images taken from centre (B) to edge (E) of the film.

The optical images clearly showed that the FSM consisted of regular array of micro cavities with few defects in the film. Near the edge the pores were not regular while the pattern became uniform on going from edge to centre. Neat polystyrene did not yield patterned film under the present experimental conditions, but irregular depressions.

The thickness of the films was measured in a stereomicroscope (*ZEISS Discovery V20DteREO*) with eye-piece and Vernier by holding the film between two glass slides. The table 5.1 provides the thickness values of the film from different volume of the PSA suspension. FSM from a volume of 0.2 ml, showed a thickness of 910 nm and the thickness gradually increased with the volume to 7.1 μm for 1.2 ml solution. The hybrid films prepared by casting different volume of PSA suspension are referred as xFSM, where 'x' represents the thickness of the film.

Table 5.1. Thickness of FSM measured by stereomicroscopy for different volume of PSA cast

Volume of PSA solution (ml)	0.2	0.3	0.5	0.7	0.9	1.0	1.2
Thickness of the film (μm)	0.91	1.5	3.0	3.9	4.8	5.6	7.1

The optical microscopic images given in figure 5.2 showed that morphological variation of the FSM occurred with the thickness of the films. A more clear picture of the morphological variation with the thickness of the films was obtained from the SEM images. Figure 5.3 shows the SEM images of the FSM of different thickness. The BF pattern was consistently uniform up to a thickness of 3.9 μm. Then it showed tendency to become more and more irregular with thickness and finally ended up in

a collapsed pattern for 7.1 µm thick film. The BF morphological features of the films were analysed by imagej and the results are summarized in table 5.2. The BF cavity

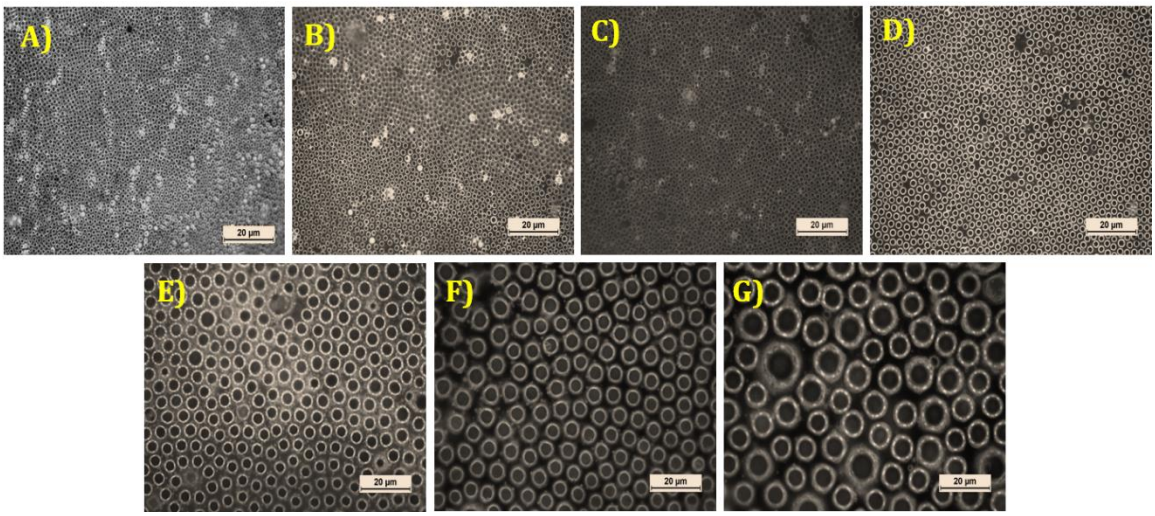

Figure 5.2. The optical microscopic images of FSM of different thickness (A) 0.91FSM, (B) 1.5FSM (C) 3.0FSM (D) 3.9FSM (E) 4.8FSM (F) 5.6FSM (G) 7.1FSM.

size and strut thickness increased while feature density gradually decreased up to the thickness of 3 µm and then the difference in the values continued to grow significantly. 0.91FSM consisted of BF cavities having average size of 0.87 µm, strut thickness of 0.66 µm and feature density of $3.06\times10^{8}/cm^{2}$. We can also observe fairly uniform distribution of concavities for 3FSM with concavities of size 2.1 µm while feature density decreased to $1.5\times10^{8}/cm^{2}$. After exhibiting a significant increase in cavity size (4.5 µm) and strut thickness (4.4 µm) for 3.9FSM, the pattern became highly irregular on increasing the thickness further. The variation in average pore size and strut thickness with thickness of the film are shown graphically in Figure 5.4. (A) and the variation of feature density in Figure 5.4. (B).

It is evident that the BF patterns with small pore size and high feature density were obtained for films having thickness ≤3µm. It may be worthwhile to note that the pattern regularity enhanced with the thickness, as can be clearly observed from

the magnified images shown figure 5.3 as insets, such that 3 μm thick film exhibited nearly hexagonal arrangement of the cavities

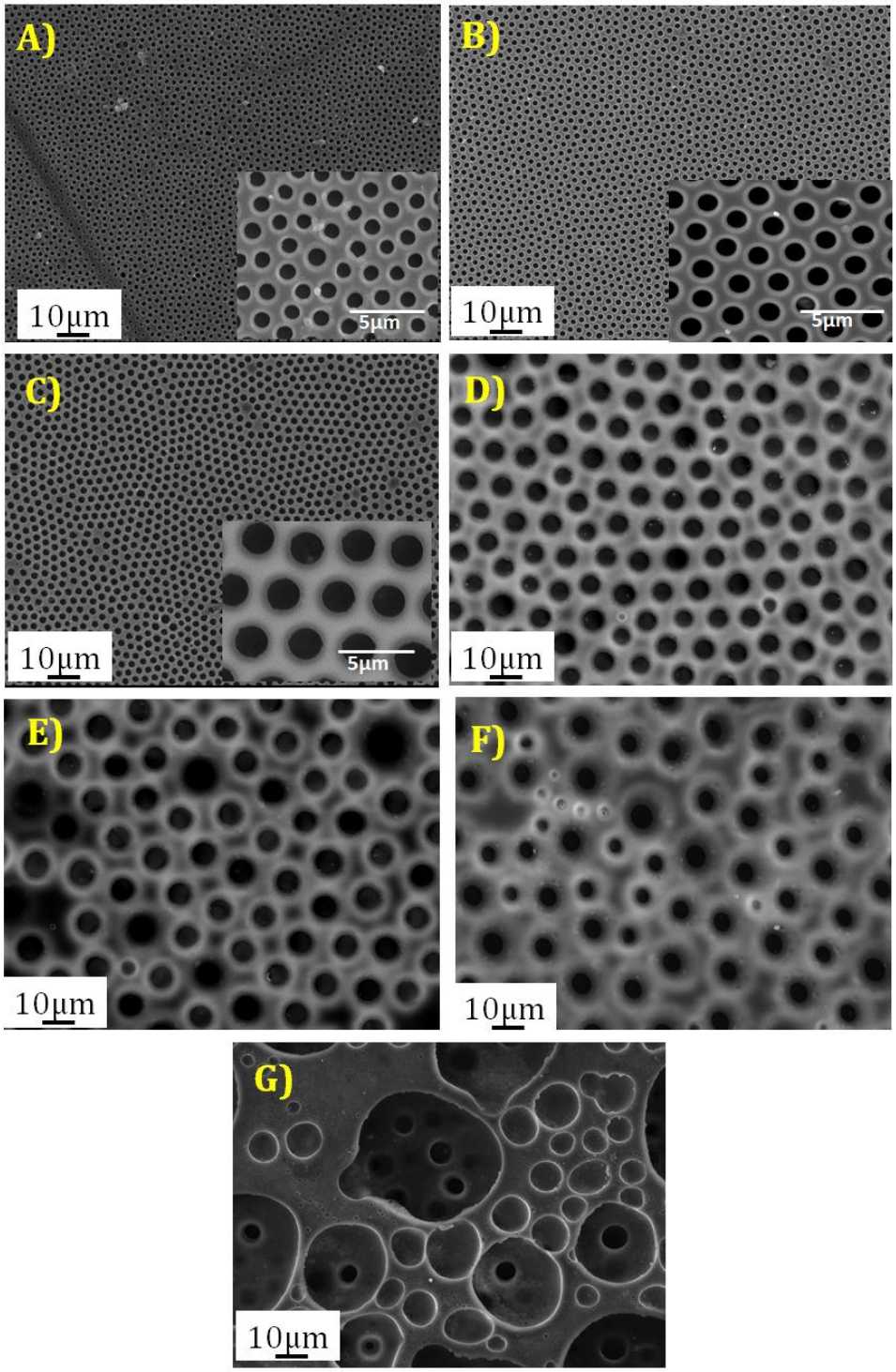

Figure 5.3. SEM images of FSM with varying thickness (A) 0.91FSM, (B) 1.5FSM, (C)3FSM (D)3.9 FSM (E) 4.8FSM, (F) 5.6FSM, and (G) 7.1FSM

Table 5.2. The size of the BF cavity, strut thickness and feature density obtained for different FSM measured using imagej

FSM	BF cavity size (μm)	Strut Thickness (μm)	Feature Density /cm^2	Conformational Entropy (S)
0.91FSM	0.87 ± 0.09	0.64 ± 0.27	3.1 × 10^8	0.68
1.5FSM	1.10± 0.08	1.00 ± 0.22	2.2 × 10^8	0.65
3.0FSM	2.10± 0.04	1.60 ± 0.17	1.5 × 10^8	0.50
3.9FSM	4.50 ± 0.17	4.40 ± 0.48	9.3 × 10^6	-
4.8FSM	3.8-5.0	3.7-7.6	9.2 × 10^6	-
7.1FSM	4-7	7-9	4 × 10^6	-

The pore size distribution of 0.91FSM, 1.5FSM and 3.0FSM films are shown in figure 5.5. It can be seen that 29% BF cavities of 0.91FSM exhibited 0.75 μm diameter (most probable diameter). The percentage of cavities exhibiting most probable diameter increased with the film thickness. The percentage of BF cavities exhibiting most probable diameter for 1.5FSM and 3.0FSM thick films were 37% and 51 % respectively.

The porosities of the films were measured by solvent penetration method. The films were weighed and then immersed in 1-butanol under vacuum for 2 hrs for the solvent to penetrate in to the pores. It was then taken out, wiped with tissue paper and immediately took the weight. The porosity in percentage was calculated from the

weight difference. The theoretically calculated true density of the hybrid material was 1.137 g/cc. Figure 5.4. (B) shows the plot of porosity against film thickness. Porosity decreased with film thickness such that the 0.91FSM film showed a high porosity of 94 % which decreased to 84.9 % for 3FSM film.

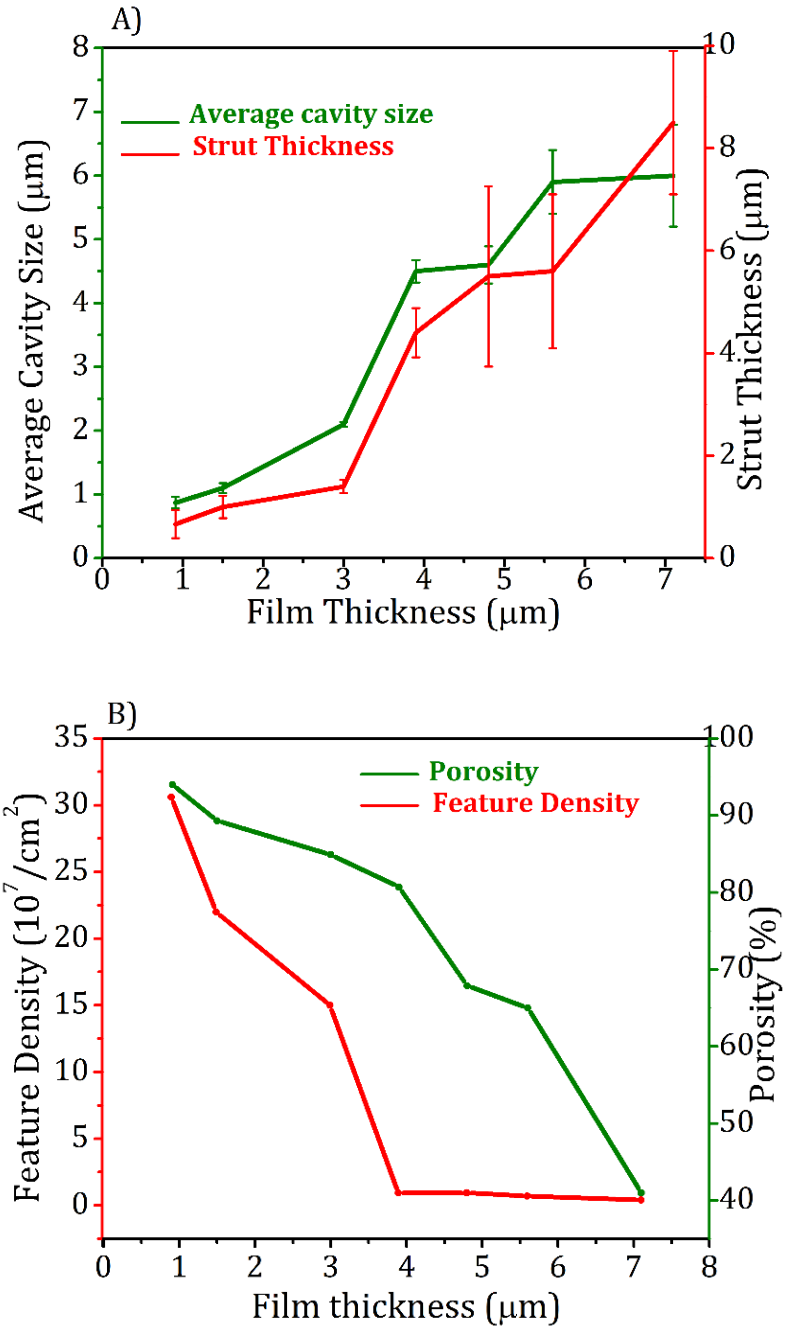

Figure 5.4. Variation of (A) Pore size and strut thickness (B) porosity and feature density of BF patterns with different thickness

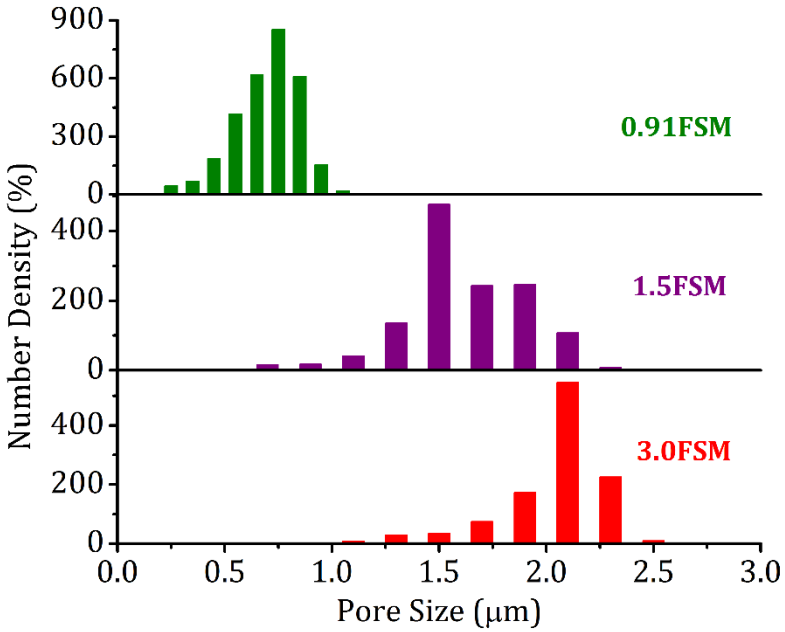

Figure 5.5. Pore size distribution of BF cavities in 0.91FSM, 1.5FSM and 3.0FSM films

5.4.1. Mechanism of BF morphology change with thickness of the film

In BF formation, time taken for the growth of the water droplets and its stabilization decides the size of the BF cavity. Steyer et al. and Knobler et al. described the growing process of water droplets on a polymer solution which involves both diffusion and coalescence (*Knobler et al., 1988; Steyer et al., 1990)*. According to them, the initial stage of droplet growth occurred as a function of $t^{1/3}$. The second stage is the coalescence dominated stage and the droplet size increases as a function of 't'. The change in exponent occurred at the last stages of BF formation because the growth at this stage was mainly due to the coalescence of the enlarged droplets. The figure 5.6 depicts the droplet growth as a function of time (adopted from *Muñoz-Bonilla et al., 2014*)

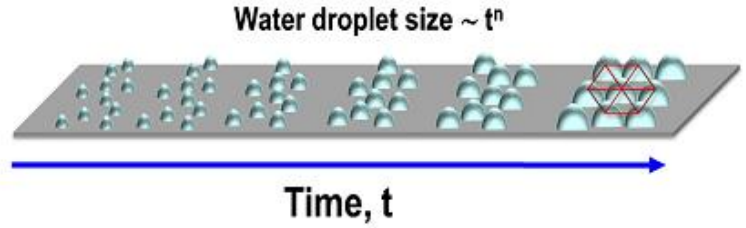

Figure 5.6. Water droplet growth as a function of time.

The droplets get stabilized when the coalescence is arrested by the precipitated polymer layer or the adsorbed inorganic particles. The ordering or the hexagonal arrangement of the droplets occurs only when significant surface coverage is achieved (*Bunz, 2006*).

BF mechanism depends on various environmental and experimental parameters described in section 1.5. *(Muñoz-Bonilla et al., 2014*). Since all the FSMs were prepared under identical conditions, the effect of environmental factors on BF formation can be ruled out. In particle-assisted BF formation, the droplets are stabilized by the adsorption of the particles at the droplet/suspension interface. Delay in stabilization will cause growth of the droplet and increase in BF cavity size. In order to understand the stabilization process in the present system, we analysed the surfaces of hybrid films with plain surfaces which were prepared by casting and drying the suspensions in a non-humid atmosphere. These films were post-treated with ninhydrin which produced dark coloured spots on the film surfaces reacting with amino groups of the particles. Figure 5.7 shows the optical microscopic images (under reflection mode) of the ninhydrin-treated films of varying thickness.

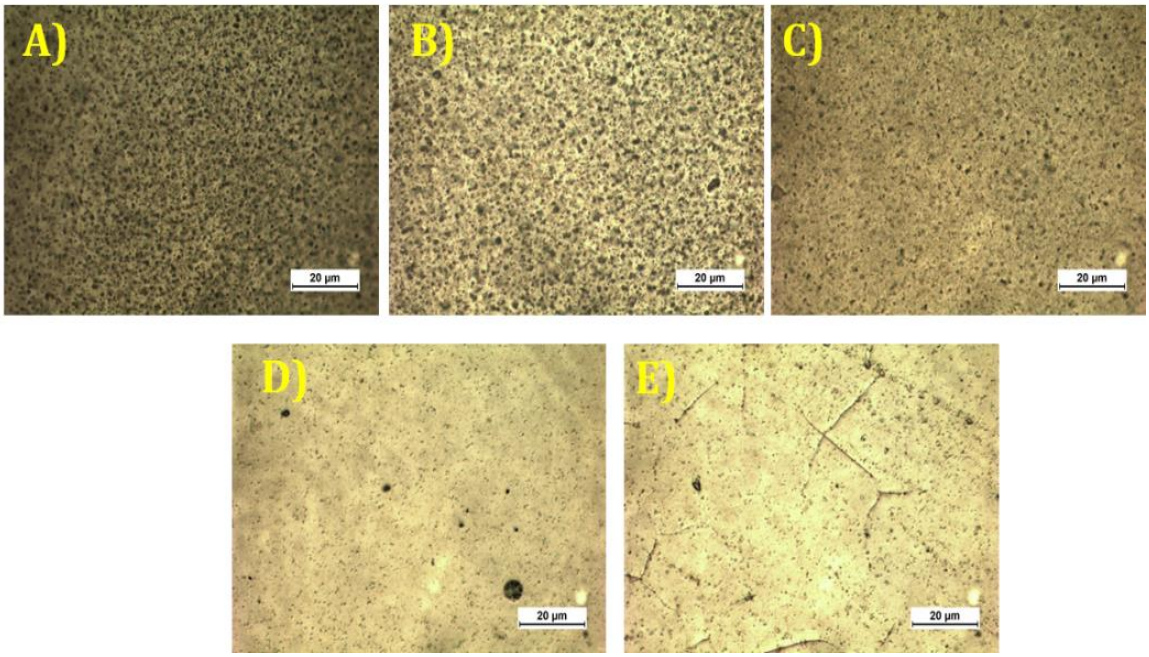

Figure 5.7. Optical images of ninhydrin-treated plain films with varying thickness (A) 0.91FSM, (B) 1.5FSM (C) 3.0FSM (D) 3.9FSM (E) 4.8FSM

The intensity of the dark shade decreased with film thickness, indicating that the concentration of the particles carried to the film surface decreased with increase in volume/height of the suspension. The particles at the film surfaces were due to the capillary flow within the suspension, induced by fast evaporation of the solvent, which carried the particles to the surface during the drying of the suspension. The reduction in the surface particle concentration could be due to the settling tendency of the particles by gravitational force and the surface particle concentration decreases with volume/height of the suspension. These particles in the surface layers, which are carried to the droplet/suspension interface by hydrodynamic drag force, are responsible for stabilization of the water-droplets. Consequently, the droplets growing on 0.2 ml suspension (0.91FSM) are stabilized first since sufficient amount of the particles are available for stabilizing the droplet. These droplets will

exhibit the lowest size and hence lowest cavity size. Increased suspension volume/height caused delay in acquiring sufficient amount of particles for stabilization. Since the droplets grow with time, the delay in stabilization facilitated the growth of the droplets further until the droplet got stabilized. Additional amount of the solvent available in the suspension for evaporation assures an environment conducive for droplet growth. The above said mechanism may explain the experimentally observed increase of BF cavity size with FSM film thickness. Although the droplets continue grow with time, growth beyond an equilibrium size causes the droplets to collapse. This could be the reason for collapsed morphology of 7.1FSM.

5.4.2. Through-pore structure in FSM

A monolayer of pores with opening in both sides of the film is referred as a through-pore structure. Such a trend was observed for 0.91FSM film. The AFM images (2D and 3D) along with the height profile shown in figure 5.8 clearly indicated the formation of through-pore structure. These openings were less regularly spaced (average spacing of ~600 nm) when compared to that of the cavity openings at the top surface (average spacing of ~400 nm) of the film. It may be noted that the BF cavity size was 0.87±0.09 μm which corresponds to droplet size. Considering the size distribution of the droplets, the droplets having size higher than the film thickness reached the substrate surface. Rupture of the film occurred at places where the droplets were in contact with the substrate surfaces, thus forming through-pores. Since the droplets of size less than the film thickness did not cause pore openings, the average spacing (~600nm) between pore-opening at the bottom surface of the film registered a higher value than of the spacing (~400nm) between the pore-opening the top surface. It may be noted that the pores were amino-functionalised due to the

presence of functionalised particles at the pore walls. The pore-openings at the bottom surface of the film had a size of ~250 nm (less than that of the size of the pore openings at the top surface) due to spherical shape of the droplets**.** Films with functionalised through-pores having micro-size opening on one side and nano-size opening at the other side can find applications in filtration of selective nanoparticles, membranes for capacitors, etc.

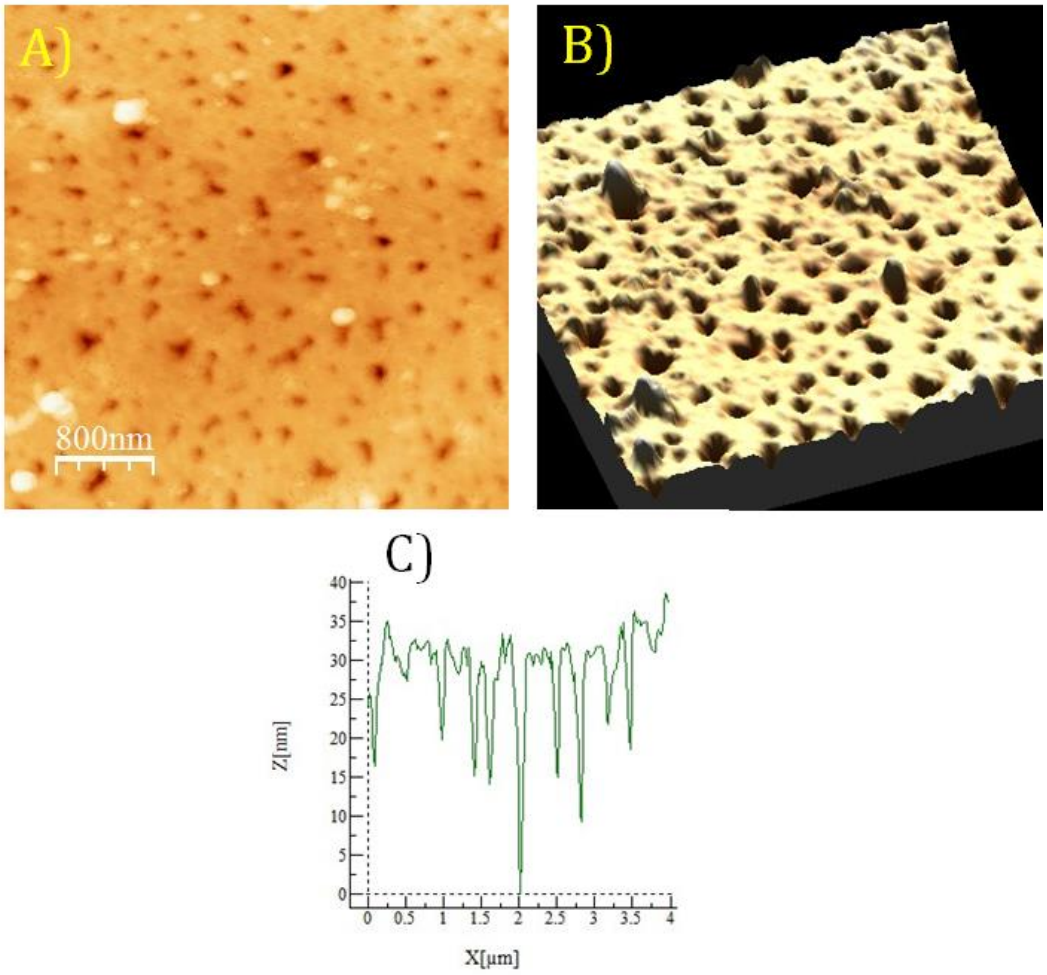

Figure 5.8. AFM images of opposite side of 0.2FSM (A) 2D and (B) 3D image (C) height profile of the pore distribution

5.4.3. Effect of particle loading on FSM morphology

FSM films having different particle concentration were also prepared for studying the effect of particle loading on BF pattern. Particle concentration was

varied in the range of 1 to 6 wt % with respect to polystyrene, fixing the suspension volume at 0.5 ml for which the film thickness was 3.0 μm. The films are referred as FSM-X%, where X% represents the particle concentration in percent by weight of polystyrene. Figure 5.9 shows the SEM images of FSM with varying particle loading. The morphological features such as pore size, strut thickness, feature density and conformational entropy of different FSM measured using imagej are presented in Table 5.4. It can be seen from the table that the cavity size and the strut thickness decreased with the increase in the particle loading from 1 % to 3 % and then increased on further increase in the particle concentration. The feature density showed the reverse trend.

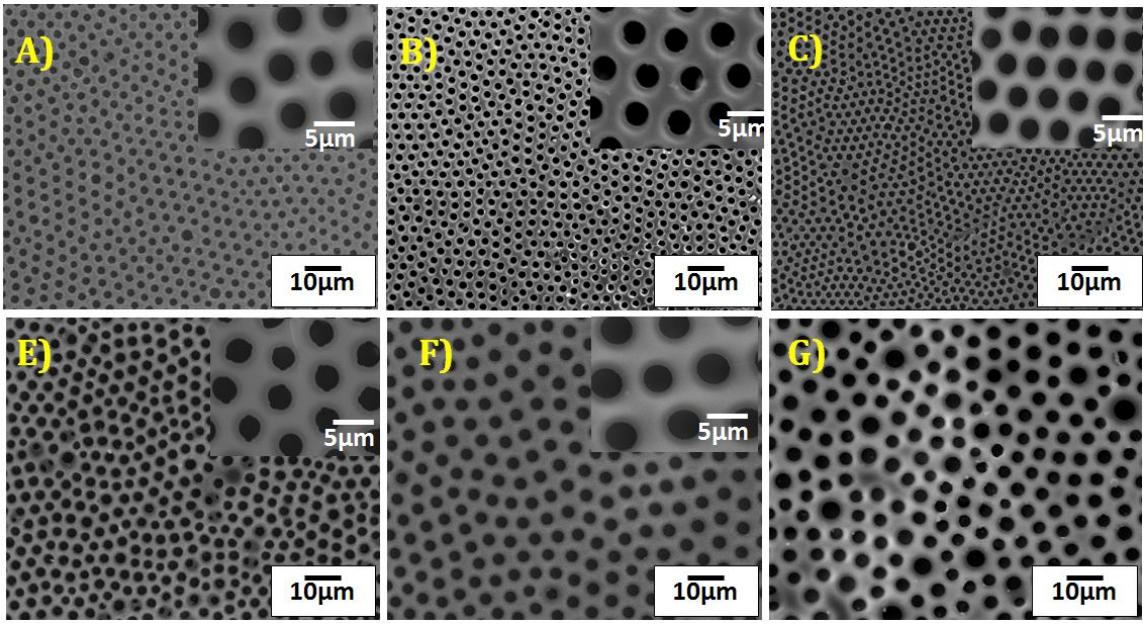

Figure 5.9. SEM images of FSM with varying particle concentration (A) FSM-1%, (B) FSM-2%, (C) FSM-3%, (D) FSM-4%, (E) FSM-5%, and (G) FSM-6%.

On the other hand, the feature density and uniformity of the pattern enhanced up to 3 wt % and then decreased/reduced with particle concentration. The minimum cavity size and strut thickness, maximum feature density and the most uniform patterns was obtained for FSM-3%.

It may be recalled that the particle dispersion-loading limit in PS matrix was 3 wt %. Obviously, cavity size minimum and feature density maximum can be expected for FSM-3% due to the availability of maximum number of particle to stabilize droplets having a size less than of the droplets on the suspensions having lesser number of particles. The same explains the decrease of the cavity size with increase of particle loading up to 3 wt %.

Table 5.3. The size of the BF cavity, strut thickness, feature density and conformational entropy obtained for different FSM with varying particles loading measured using imagej

FSM	Pore size (μm)	Strut thickness (μm)	Feature density(/cm)	Conformational Entropy (S)
FSM-1%	2.7 ± 0.06μm	2.1 ± 0.23μm	6.8×10^7	0.63
FSM-2%	2.5 ± 0.05μm	1.8 ± 0.23μm	10.9×10^7	0.55
FSM-3%	2.1±0.08 μm	1.6 ±0.14 μm	$15 .0\times 10^7$	0.50
FSM-4%	2.4±0.08 μm	1.6 ±0.16 μm	7.4×10^7	0.62
FSM-5%	3.1±0.09 μm	3.0 ±0.52 μm	3.5×10^7	0.74
FSM-6%	4.0±0.22 μm	3.7 ±0.57 μm	1.5×10^7	-

On the other hand, particle loading above the particle dispersion-loading limit of 3 wt % led to particle-agglomeration. This resulted in the reduction in effective number of particle domains thereby increasing the droplet size in FSM film containing particle loading above 3 wt %. However, it may be interesting to note that FSM film with particle loading up to 5 wt % retained moderately ordered patterns in contrast to that observed for drop-cast films (Section 3.4.2.). In drop-cast films, the

pattern was sensitive to particle loading such that ordered pattern was observed only at particle dispersion-loading maximum, i.e. for the film with particle concentration at particle dispersion-loading limit of 3 wt %.

This can be explained in terms of the difference in the volume of the suspension used for covering unit area to produce uniform BF pattern in drop-cast and FSM films, the total amount of the dispersed particles available per unit area for the stabilization of the droplets, and sensitivity of the suspension to the change in particle concentration with respect to the amount of particle required for producing uniform pattern in unit area. The drop-cast film and the FSM films under discussion were prepared from suspension volume of 3 μL and 0.5 ml respectively. Whereas drop-cast suspension spread an area of approximately 1cm^2, the suspension for FSM film was spread in an area of 3.5 cm^2. i. e. the suspension volume per unit area was 3 μL and 0.16 ml respectively. In fact, the total amount of particles available in 3μL suspension with 3 wt % particle (dispersion loading limit of the particle) is sufficient for producing regular BF patterns per unit area. Consequently, the total amount of particles per unit area available for preparing FSM film is ~53 times in excess of the required amount for producing regular BF pattern. The FSM films under consideration were prepared using suspensions containing 1-5 % particles. Considering that uniform BF pattern by drop-casting was produced by 3 wt % suspension, the change that brought in particle concentration was less than ±2 times, which is insignificant when compared to the availability particles in the suspension of FSM film. This may account for the occurrence of the almost similar patterns in FSM film from suspensions of particle concentration in the range of 1-5 wt %. However, surface layers of the suspensions can be affected by reducing the

suspension concentration below 3 wt %. Similarly, particle-agglomeration above the dispersion-loading limit (3 wt %) also bring reduction in the concentration of dispersed particles. The effect of particle-agglomeration becomes more and more pronounced as the particle loading increases. This may explain the increase of BF cavity size in films on deviating the particle concentration from 3 wt %.

5.4.4. Effect of using 2.2SA31 particles

The drop casted films prepared from SA31 particles (the particles treated with AS/VS ratio of 3:1) described in chapter 3 could not produce regular BF patterns on the PS surfaces as that with SA11 particles. Figure 5.10 shows the microstructure of the FSM film prepared from 2.2SA31 suspension in PS/chloroform solution by casting 0.2 and 0.5ml suspension. These films are referred as 0.2FSM-31 and 0.5FSM-31 respectively. The microstructure indicated that, the uniformity is still a question. As expected, the average pore size increased from 0.2FSM-31 (1.2 μm) to 0.5FSM-31 (3.1 μm) and feature density decreased from 2.3×10^8 to $5.2\times10^7/cm^2$. The higher cavity size of FSM-31 with respect to FSM-11 was due to the higher percentage of hydrophilic amino groups per particles which facilitates particle adsorption at the water droplet/polymer solution interface.

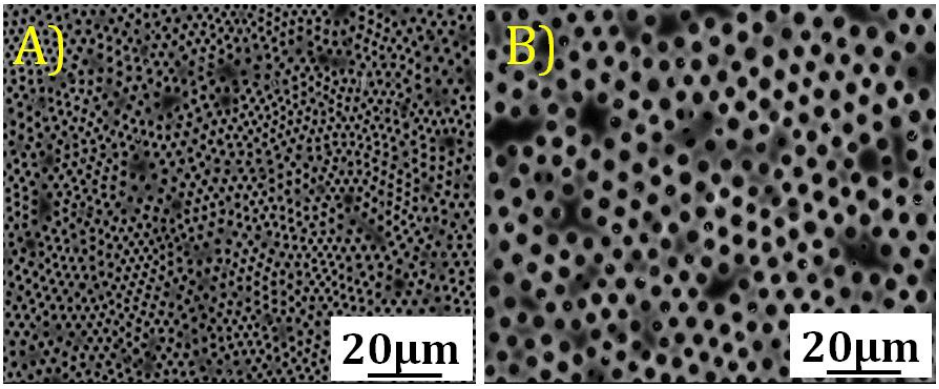

Figure 5.10. SEM images of (a) 0.2FSM-31 (b) 0.5FSM-31

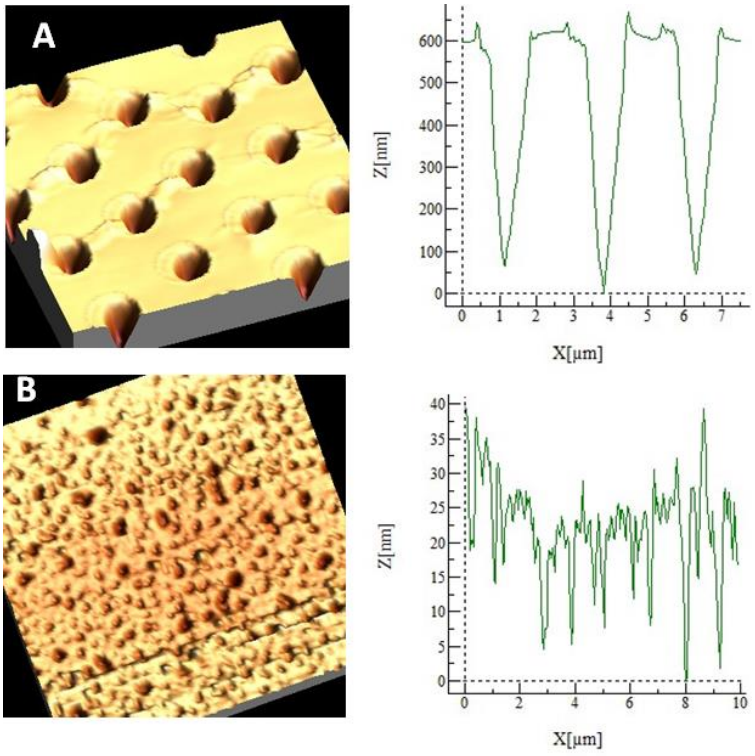

Figure 5.11. 3D-AFM images of 0.2FSM-31 (A) front side (B) Opposite side along with the height profile

0.2FSM-31 film also produced through-pore structure, as was observed for 0.2FSM-11 film, and confirmed from the AFM images (figure 5.11), but with higher percentage of through-pores than 0.2FSM-11 film. This could be due to the improved hydrophilicity of SA31 particles, containing higher percentage hydrophilic amino group than in SA11 particles, which facilitated penetration of the water droplets into the suspension during formation of breath figures.

5.4.5. Amino-functionalised BF cavities of FSM film

The amino-functionalized cavities were proven by the treatment with fluorescamine as described chapter 3. Figure 5.12 shows the fluorescent images of FSM films 0.91FSM, 1.5FSM and 3.0FSM. The functionalization of BF cavities of FSMs

with the amino group was evidenced by the presence of fluorescent rings on the fluorescamine treated films on excitation with red light.

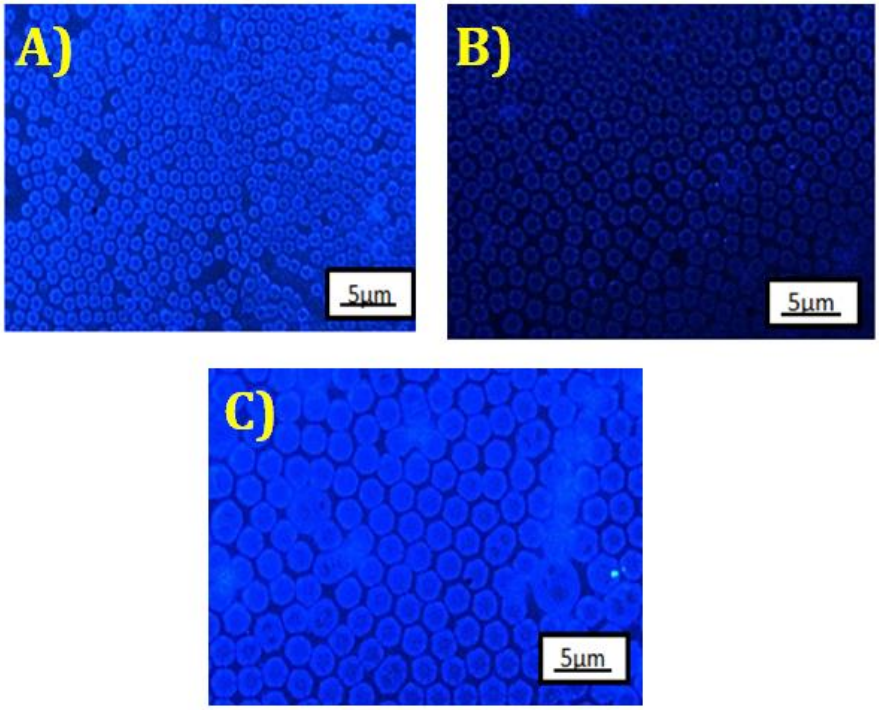

Figure 5.12. Fluorescence microscopic images of FSM (a) 0.91FSM (b) 1.5FSM and (c) 3.0FSM after treatment with fluorescamine

The quantification of amino groups in the cavities was evaluated by fluorescence spectroscopic analysis using Spex-Fluorolog FL22 spectrofluorimeter equipped with a double grating 0.22 m Spex 1680 monochromator, and a 450 W Xe lamp as the excitation source and a Hamamatsu R928P photomultiplier tube detector. The film state spectra were recorded by front phase mode. The fluorescamine treatment on FSM for fluorescence analysis were carried out as described in chapter 3. Figure 5.13(A) & (B) shows the fluorescent spectra of fluorescamine treated FSM films with varying thickness and varying particle concentration. The strong fluorescent adduct formed by the reaction between fluorescamine and the amino group on the alumina particles which were located

inside the BF cavity produced a broad and blue fluorescence (~450nm) at room temperature. Hence, the fluorescent intensity of the peaks corresponds to the quantity of amino functionality present on the different FSM films. Figure 5.13(A) shows that the intensity of the peak decreased with increase of the FSM film thickness. In other words, 0.91FSM showed the maximum density of amino functionality in the BF cavities followed by 1.5FSM and 3.0FSM. The maximum density of amino functionality with 0.91FSM can be attributed to the relatively large surface area of the film due to the high feature density.

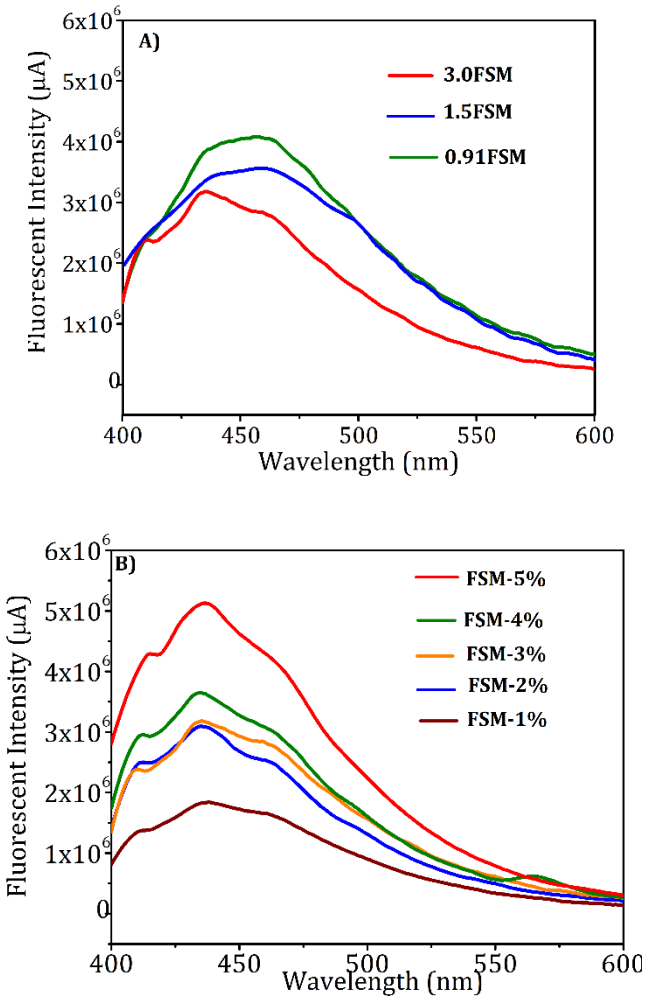

Figure 5.13. Fluorescence absorption spectra of FSM films with (A) varying thickness (B) varying particle loading

The shift in the peaks to lower wave length with thickness of the film is due to the increase in the cavity size with film thickness and hence, required of more energy to excite the electron from the amino-dye adduct. The florescence intensity of FSM film also increased with the increase in particle concentration. FSM with particle loading of 5 wt % showed the maximum intensity of 5.1×10^6 μA although it showed a lower feature density. This might be due to the maximum particle content of the cavity walls. In other words, the particle packing density on the cavity walls increases with particle loading.

The enrichment of amino functionalities inside the cavity via one step breath figure approach has many advantages in biological and biotechnical fields owing to the ease of modification of the active amino group. The amino functionality inside the BF cavity of FSM hybrid films facilitates the selective immobilization of biomolecules to even other inorganic nanoparticles (*Zhang et al., 2007*).

5.4.6. Thermal and mechanical properties

Nanoindentation is the most recent development to measure the mechanical properties of nanocomposites thin films. The quantitative evaluation of the hardness and modulus of the thin films is possible by depth sensing indentation measurements, which provides insight into the materials' response to controlled deformation at small scales. Combining the information obtained from the indentation data and the topography of the indented area using scanning force microscopy (SFM), atomic force microscopy (AFM) or optical microscopy (OM), it is possible to measure the true contact area and subsequently recalculate the hardness with accuracy. The thin film is deposited on a hard substrate for the indentation analysis and the topographical analysis gives significant information regarding the

response of the system to the indentation at nanometer scale (*Randall et al., 2002*). The load-displacement curve obtained from the depth-sensing indentation aids to calculate the quantitative values of hardness and modulus. The material parameters like hardness and modulus can be calculated from residual contact area of the indent by the following equations(*Oliver et al., 1992*).

$$\boldsymbol{H = \frac{P}{A}} \qquad \textbf{---------- (5.1)}$$

$$\boldsymbol{E_{eff} = \frac{E}{1-\nu^2} = \frac{\sqrt{\pi}}{2}\frac{S}{\sqrt{A}}} \qquad \textbf{---------- (5.2)}$$

Where 'P' is the load, 'A' is the projected contact area, 'E_{eff}' is the effective elastic modulus, 'E' is the Young's modulus, 'ν' is the Poisson's ratio, and 'S' is the experimentally measured contact stiffness.

Nanoindentation measurements on FSM films were carried out using an Anton Paar Table Top standard Nanoindentation Tester (NHT). (Generally, the test procedures are not included in thesis) The system has a load and displacement resolution of 1N and 0.3nm respectively. The load for indentation was varied from 0 to 1mN.

The load-displacement curve obtained for FSM films and the neat polystyrene films with plain surfaces (UP film) are shown in figure 5.14 (A) and (B). In the case of UP films, the depth of indentation (h_{max}) decreased with the particle loading while FSM films showed a different trend. The depth of indentation on FSM-1% and FSM-3% was higher than on the UP film. However, FSM-5% showed a remarkable resistance to indentation indicated by the lower indentation depth value when compared to that of PS film. It is interesting to note that FSM-1% and FSM-3% relaxed far more than UP film and FSM-5%, which was evidenced from the load-displacement profile where $h_{max} >> h_f$ (the final displacement). This might be due to the fact that BF

patterns on FSM-1% and FSM-3% films imparted a cushion effect to the film. Whereas the FSM-5% film restricted the relaxation as the high particle concentration in the

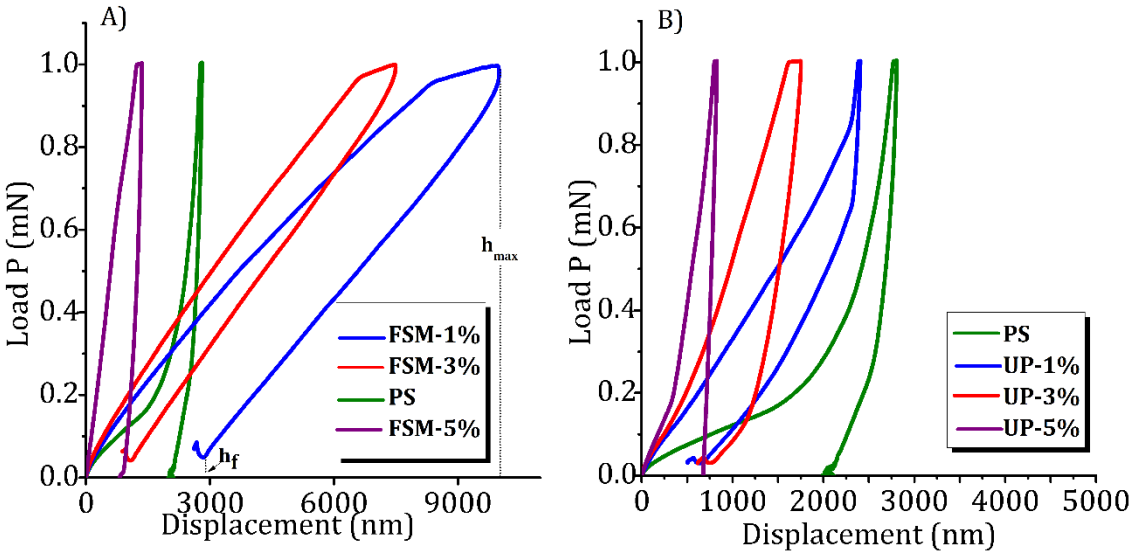

Figure 5.14. Load –displacement curve obtained after the Nanoindentation experiments performed on (A) FSM and (B) unpatterned (UP) film by applying load from 0-1 mN.

BF cavities dispersed the load and the film exhibited enhanced hardness. Figure 5.15 shows the optical images of the residual imprint of nano-indentation on the UP, FSM-5% and UP-5% films respectively. The hardness and elastic moduli values of these films were calculated from the load-displacement curve and graphically shown in figure 5.16 (A) and (B). It can be seen from the plots that the hardness and moduli increased with particle content. The PS film showed a hardness and moduli of 5.6 MPa and 0.05 GPa respectively. The average hardness and moduli of UP hybrid films increased from 9 to 71 MPa on increasing the particle loading from 1 to 5 wt %. Similarly, the Young's moduli increased from 1.02 to 2.5 GPa with the particle content. The FSM films also showed an analogous increase in the value of hardness as well as Young's Moduli with the particle loading. The hardness values for the FSM-

1%, FSM-3% and FSM-5% were 1.19 MPa, 4.06 MPa and 26.7 MPa respectively. Corresponding Young's moduli values were 0.1 GPa, 0.42 GPa and 0.98GPa. The lower hardness and stiffness for FSM-1% and FSM-3% compared to that UP film can be due

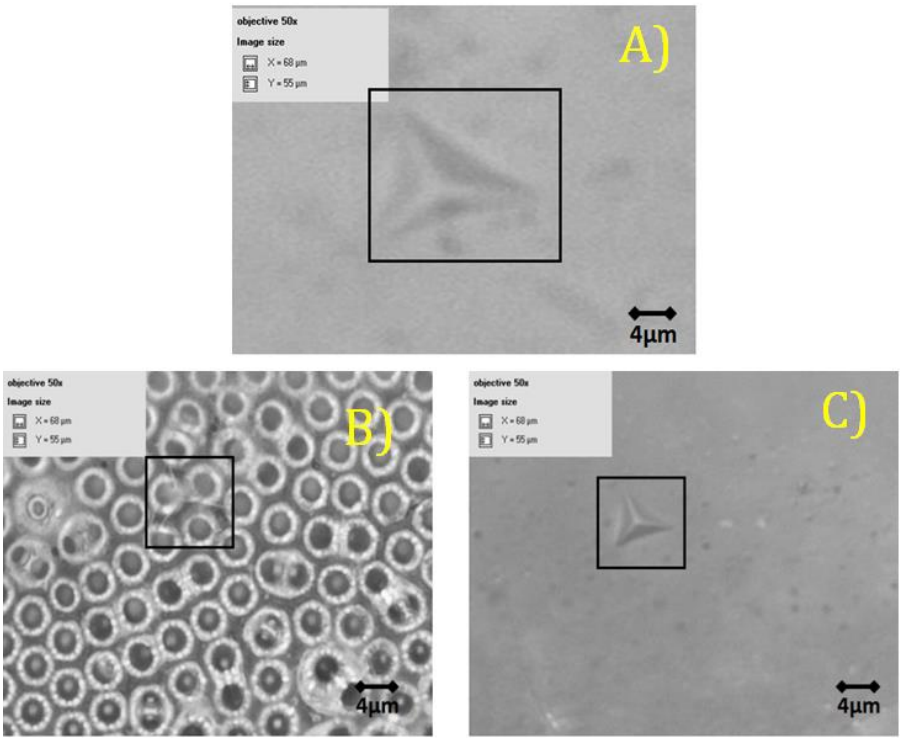

Figure 5.15. Optical images of residual imprint of nanoindentation performed on (A) polystyrene film, (B) FSM-5% and (C) UP-5%.

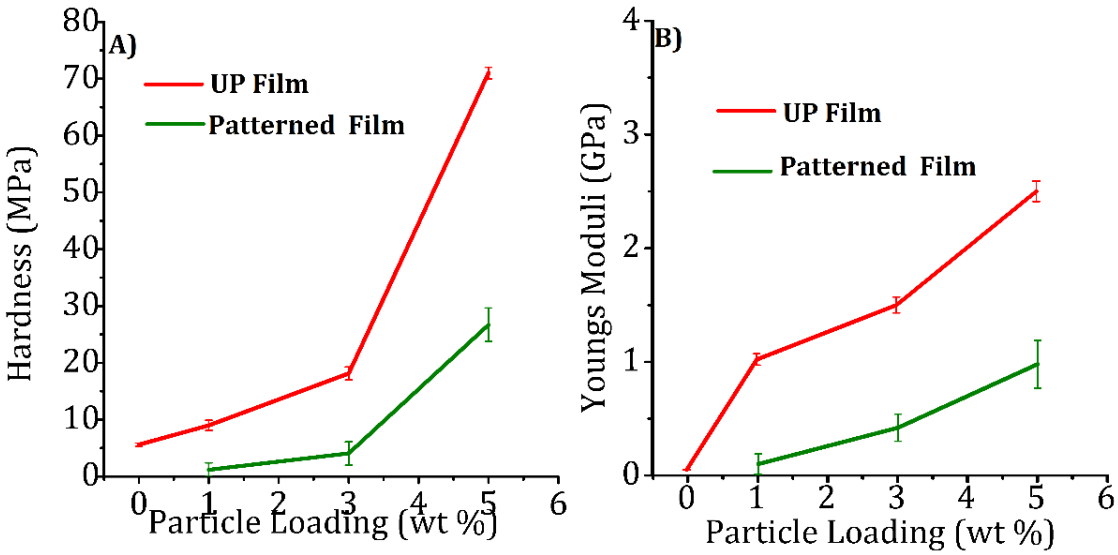

Figure 5.16. Variation of (A) hardness and (B) Young's moduli of UP films and FSM films of different particle loading in comparison polystyrene film

to porosity in the cavity walls whereas in FSM-5% the property improvement by closely packed particles over-rides the adverse effect of porosity**.** The improved handling properties of the film due to enhanced stiffness and harness would useful during applications

FSM films showed higher thermal stability up to 360°C compared to the polystyrene which decomposes at 280 °C. Figure 5.17. shows the TG curve of FSM films along with commercial polystyrene by heat treatment up to 500 °C. The composites prepared from the different concentration of SA particles showed the corresponding weight percentage of inorganic content. There is a shift in the decomposition temperature for 50% (T_{50}) and 100% (T_{100}) weight loss for FSM compared to PS. T_{50} shifts in the order of 397 °C for PS, 412 °C for FSM-3% and 435 °C for FSM-5%. Similarly, T_{100} values are 415 °C for PS, 435 °C for FSM-3% and 457 °C for FSM-5%.

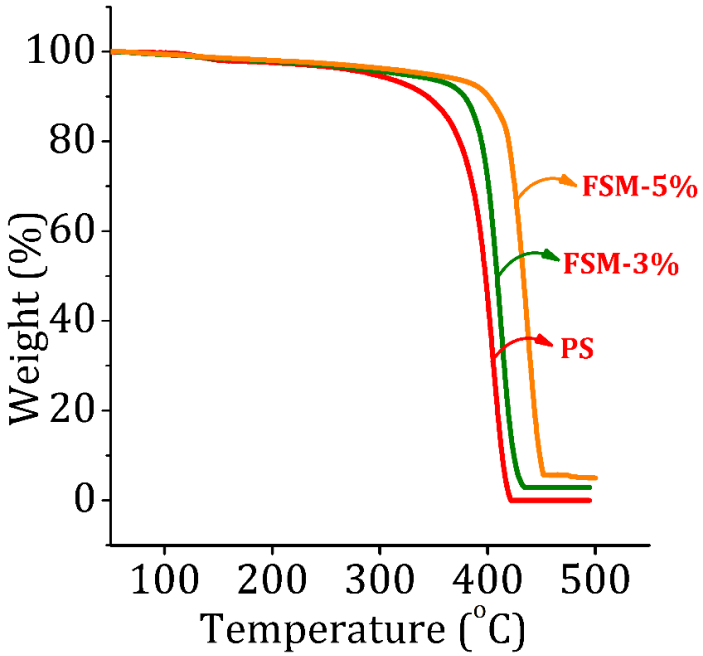

Figure 5.17. TG curves of FSM films at different particle loading along with the polystyrene

5.5. CONCLUSIONS

Free-standing micropatterened polystyrene-alumina hybrid films with amino functionalized BF cavities (FSM) were fabricated from suspensions of the functionalised particles in polystyrene/chloroform solutions by a simple casting method. Amino-functionalised amphiphilic-alumina particles having Hb/Hp ratio of 4 was used for the purpose. Casting and drying of the suspension in glass petri-dish produced micropatterned film which came off from the container on pouring methanol over the film. The cavity size increased while feature density decreased with increase of the thickness of the film. The morphological variation was explained in terms of solvent evaporation time from different volumes of the suspensions. Increased evaporation time with increased suspension volume caused enhanced cavity size. A through-pore structure has been formed on 0.91FSM which find applications in selective filtration of nanoparticles. The morphological variation with the particle loading was also studied and found that uniform concavities with high feature density was formed at a particle loading of 3 wt %.

The quantitative estimation of amino groups present inside the BF cavity of FSM was carried out by fluorescence spectroscopic analysis of the fluorescamine treated FSM. The study revealed that the fluorescence intensity which is corresponding to the percentage of amino functionality increases with the thickness of the film as well as with the particle loading. Similarly, FSM showed an enhanced mechanical strength and thermal stability. FSM-5% exhibited a high percentage of amino functionality (fluorescent intensity = 5.1×10^6 μM), enhanced mechanical strength (hardness =26.7MPa), and a good thermal stability (T_{100} = 456°C). Here, we were succeed in fabricating amino functionalised free-standing micropatterend

hybrid film with enhanced mechanical strength and thermal stability which can have wide range of applicability in many industrial and biological fields.